



**HAL**  
open science

## New developments of a fission chamber for very high radioactivity samples

B. Laurent, J. Taieb, G. Bélier, Paola Marini, P. Morfouace

► **To cite this version:**

B. Laurent, J. Taieb, G. Bélier, Paola Marini, P. Morfouace. New developments of a fission chamber for very high radioactivity samples. Nuclear Instruments and Methods in Physics Research Section A: Accelerators, Spectrometers, Detectors and Associated Equipment, 2021, 990, pp.164966. 10.1016/j.nima.2020.164966 . hal-03368961

**HAL Id: hal-03368961**

**<https://hal.science/hal-03368961>**

Submitted on 7 Oct 2021

**HAL** is a multi-disciplinary open access archive for the deposit and dissemination of scientific research documents, whether they are published or not. The documents may come from teaching and research institutions in France or abroad, or from public or private research centers.

L'archive ouverte pluridisciplinaire **HAL**, est destinée au dépôt et à la diffusion de documents scientifiques de niveau recherche, publiés ou non, émanant des établissements d'enseignement et de recherche français ou étrangers, des laboratoires publics ou privés.

1 New developments of a fission chamber for very high  
2 radioactivity samples

3 B. Laurent<sup>a,b,\*</sup>, J. Taieb<sup>a,b</sup>, P. Marini<sup>a,1</sup>, P. Morfouace<sup>a,b</sup>, G. Bélier<sup>a,b</sup>

4 <sup>a</sup>CEA, DAM, DIF, F-91297 Arpajon, France

5 <sup>b</sup> Université Paris-Saclay, CEA, LMCE, 91680 Bruyères-le-Châtel, France

---

6 **Abstract**

A new fission chamber was developed and built for prompt-fission-neutron spectra (PFNS) measurements in neutron-induced fission of actinides, and is described in J. Taieb *et al.*, Nucl. Instr. and Meth. A 833 (2016) 1-7. It allowed us to minimize incident- and outgoing-neutron scattering, and optimize both time resolution and alpha to fission fragment discrimination. The fission chamber was validated and used for <sup>238</sup>U and <sup>252</sup>Cf PFNS measurements. To measure PFNS of samples with a natural alpha activity of the order of 10 MBq, further improvements to the detector were done and are presented in this work. Tests of the improved fission chamber lead to a fission fragment detection efficiency of 91% for a 14.41 MBq <sup>240</sup>Pu deposit, and 99% for a 247 kBq <sup>242</sup>Pu deposit. The fission chamber was successfully used for <sup>239</sup>Pu PFNS measurements at the Weapons Neutron Research facility of the Los Alamos Neutron Science Center (WNR@LANSCE).

7 *Keywords:* Fission chamber, high activity samples, efficiency, segmented  
8 anode

---

9 **1. Introduction**

10 In recent publications [1, 2], a new type of light-weighted fission chamber  
11 developed for Prompt-Fission-Neutron Spectra (PFNS) measurements was pre-  
12 sented. Actinide mass, time resolution and the amount of structural material  
13 were optimized to improve both alpha-fission fragment discrimination and time-  
14 of-flight measurements resolution, as well as to reduce the amount of neutrons

---

*Corresponding author*

*Email address:* benoit.laurent@cea.fr (B. Laurent)

<sup>1</sup>Present address: CENBG, CNRS/IN2P3-Université de Bordeaux, Chemin du Solarium  
B.P. 120, 33175 Gradignan, France

15 scattered from the detector. These chambers were successfully used in PFNS  
16 experiments at different facilities: LICORNE at Institut de Physique Nucléaire  
17 Orsay (IPNO), Weapon Nuclear Research (WNR) at Los Alamos, 4MV Van  
18 de Graaff at Bruyères-le-Chatel. Some results on  $^{238}\text{U}(\text{n},\text{f})$  reactions were pub-  
19 lished [2, 3].

20 The next step was to use the fission chamber in experiments using high  
21 alpha-activity actinides such as  $^{239}\text{Pu}$ . While the main principle of the detector  
22 remains the same (gas type and pressure, gap between anode and cathode),  
23 improvements are needed to deal with the high activity of the sample in terms  
24 of radioprotection on one hand, and to avoid alpha-signals pile-up, which de-  
25 grades the alpha-fission fragment discrimination, on the other. By improving  
26 this discrimination, cuts on angular and energy distributions of detected fis-  
27 sion fragment are reduced and the induced bias on extracted PFNS and others  
28 observables (angular distribution, mean neutron energy, number of neutrons  
29 emitted per fission...) become negligible. In the following, details of the de-  
30 tector developed for  $^{239}\text{Pu}$ , but well suited for any other high alpha-activity  
31 sample, will be presented.

## 32 **2. New design of the chamber**

### 33 *2.1. Mechanical aspects*

34 A schematic view of the fission chamber is shown in Fig. 1. As for the  
35 chamber described in [1], the material budget was minimized, to ensure low  
36 neutron-scattering rate, thus reducing the neutron background generated dur-  
37 ing the experiment. Following the same idea, all used materials are almost  
38 hydrogen-free. However, because of the high activity of the  $^{239}\text{Pu}$  deposits, han-  
39 dling and assembling the targets in the chamber had to be performed in gloves  
40 box. Therefore, the external case of the  $^{239}\text{Pu}$  detector had to be redesigned to  
41 take into account this specificity. Moreover, the dimensions of the detector were  
42 increased so that structural material does not intercept the neutron flight path.

43 When in use, the fission chamber is filled with flowing tetrafluoromethane  
44 ( $\text{CF}_4$ ) gas at a fixed absolute pressure typically 100 mbar above atmospheric  
45 pressure.

46 The external structure is a 1 mm-thick aluminium parallelepiped soldered on  
47 a 4 mm-thick aluminium flange. The structure supports glued titanium foils on  
48 each side: 100  $\mu\text{m}$  thick on rectangular sides, 50  $\mu\text{m}$  thick on entrance and exit  
49 sides. Titanium foils are glued from the inner side, to stand the gas pressure  
50 inside the chamber. The soldered flange is screwed on the flange glued to the  
51 PCB. An o-ring ensures the gas tightness between the cover and the PCB.

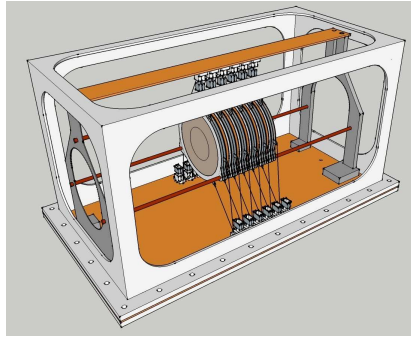


Figure 1: *Scheme of the assembled fission chamber (titanium foils are not shown).*

52 All the electronic connections and mechanical support were placed on the  
53 bottom side of the chamber. This side consists in a printed circuit board (PCB)  
54 supporting all front-end electronics components. The anodes are connected on  
55 the internal side, while pre-amplifiers are connected on the external one. The  
56 PCB also integrates high voltage connections for the drift field between anodes  
57 and cathodes, low voltage connections for pre-amplifiers and a readout connector  
58 for each anode. A 3 mm-thick aluminium flange is glued on the external face  
59 of the PCB to fix the cover. Aluminium structures fixed on the internal face of  
60 the PCB supports three rods made of Torlon® [4] to position the electrodes.

61 *2.2. The cathodes*

62 Twenty-two  $^{239}\text{Pu}$  samples were prepared by the JRC-Geel target laboratory.  
63 The sample thickness is a compromise between the amount of matter (and thus  
64 the fission rate) and the energy loss of the emitted fission fragments in the  
65 deposit. The lower the loss, the better the alpha-fission fragment discrimination.

66 The Plutonium material was electroplated on a  $25\ \mu\text{m}$ -thick aluminium back-  
67 ing (see Fig. 2), glued on the cathode frame. The diameter of the deposit is  
68  $33\ \text{mm}$  with a thickness of  $250\ \mu\text{g}/\text{cm}^2$ . Each deposit contains  $\approx 2.1\ \text{mg}$  ( $5\ \text{MBq}$ )  
69 of  $^{239}\text{Pu}$  for a total of  $47\ \text{mg}$  housed in the chamber. The ground connexion of  
70 the cathode to the chamber is ensure by a glued cable.

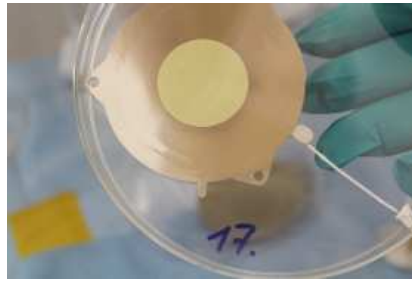


Figure 2:  $^{239}\text{Pu}$  sample electroplated on the cathode frame, with glued cable for the ground connexion in the detector.

71 *2.3. Fission chamber assembly*

72 The mounting of the Pu deposits inside the fission chamber was performed  
73 at JRC-Geel in a dedicated gloves box. The PCB with internal supports was  
74 positioned vertically and then cathodes, spacers and anodes were threaded on  
75 the insulating rods (see picture 3(a)). Each anode collects the signal from two  
76 deposits (cathodes): one on each side. So there are 11 electronics channels  
77 corresponding to the 22 deposits.

78 Once the 22 cathodes and the 11 anodes are installed, the chamber is closed  
79 by the cover (picture 3(b), right), and it can be removed from the gloves box  
80 after contamination clean-up.

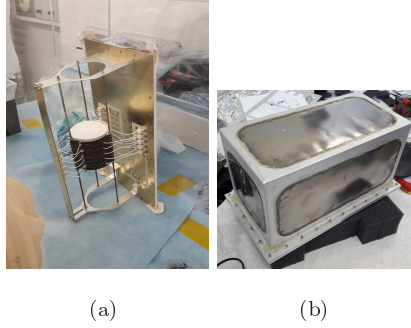


Figure 3: Pictures of the fission chamber assembly in a gloves box. The stack of anodes and cathodes (with  $^{239}\text{Pu}$ ) is mounted (a) before closing the detector with the cover (b).

### 3. Dedicated segmented anodes

#### 3.1. Anode principle

One anode of the fission chamber deals with 10 MBq alpha activity compared to a standard fission rate during experiments of around 15 f/s. In order to improve alpha-fission fragment discrimination, a dedicated anode was designed. The goal is to reduce the impact of alpha pile-up on the detection of fission fragments and enhance their discrimination. As the alpha-fission fragment discrimination is based on the different charge-signal amplitudes induced by alpha particles and fission fragments, the worst scenario occurs when an alpha is emitted parallel to the cathode. Indeed in this case its deposited charge is close to the one deposited by a fission fragment emitted perpendicularly to the cathode. The alpha-particle track length can be longer than the radius of the anode (37 mm), while the track length of the fission fragment will be only the gap between the anode and the cathode (2.5 mm), as shown in Fig. 4(a). The anode was therefore segmented in two concentric regions and the collected charge was read only from the central zone. This allowed us to reduce the amount of alpha signals with amplitudes comparable with the ones from fission fragments. The external part of the anode is isolated from the central part but kept at the same

99 electrical potential, so not to distort the electric field in the collection region.

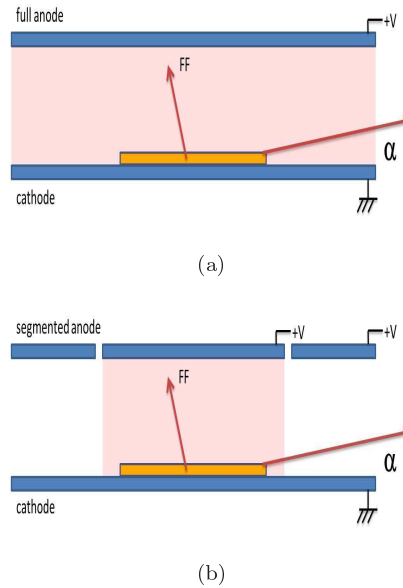


Figure 4: *Principle of the segmented anode. The red zone corresponds to the charge collection zone. In case of a full anode, alphas and alphas pile-up can have greater amplitudes than fission fragments (FF) ones (a). With the segmented anode, this amplitude is reduced (b).*

100 Moreover, a dedicated modern front-end electronics with very short shaping  
 101 times ( $\approx 10$  ns) also reduces the signals pile-up and improve the time resolution  
 102 of the setup.

103 This peculiar anode design, suitable for high-activity samples fission cham-  
 104 ber, have been patented [5].

### 105 3.2. Validation tests with high alpha-activity $^{240,242}\text{Pu}$ deposits

106 This new anode concept was tested with high alpha-activity deposits of  
 107  $^{240,242}\text{Pu}$ . These two isotopes are characterized by a very high alpha-activity  
 108 compared to their spontaneous fission decay rate. They are then good can-  
 109 didates to test offline the limits of alpha-fission fragment discrimination. A

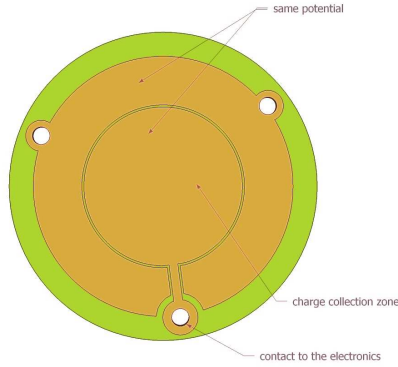


Figure 5: *Segmented anode scheme.*

110 14.41 MBq- $\alpha$   $^{240}\text{Pu}$  and 0.247 MBq- $\alpha$   $^{242}\text{Pu}$  deposits were mounted alternatively  
 111 in the chamber, equipped with plain and then segmented anodes to quantify the  
 112 improvements. The other characteristics of the chamber were kept constant (gas  
 113 pressure, gap between anode and cathode, electric field, electronics, DAQ sys-  
 114 tem). Fig. 6 and 7 show the pulse-height spectra collected for these deposits  
 115 when using a plain anode.

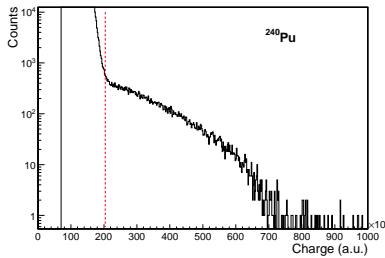


Figure 6: *Pulse height spectrum of the  $^{240}\text{Pu}$  sample (14.41 MBq), with a fission event detection efficiency of 66%. The red dotted line show the threshold used to determine the number of detected fission fragments.*

116 Because of the deposits thickness ( $0.24 \text{ mg/cm}^2$ ), some of the fission frag-  
 117 ments are stopped in the deposit. Monte-Carlo simulations [6] showed that

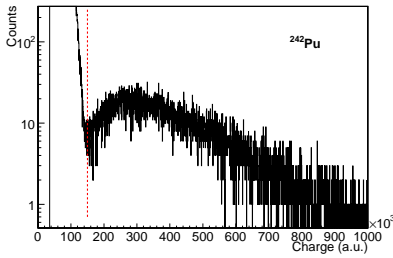


Figure 7: Pulse height spectrum of the  $^{242}\text{Pu}$  sample (0.247 MBq), with a fission event detection efficiency of 97%. The red dotted line show the threshold used to determine the number of detected fission fragments.

118 fission fragments have an efficiency of 94% to exit the deposits with enough en-  
 119 ergy to be detected in the gas afterwards. This loss has to be taken into account  
 120 in the fission detection efficiency calculation.

121 To improve the alpha-fission fragment discrimination, the time signal of the  
 122 anode was integrated over two gates and a pulse-shape discrimination (PSD)  
 123 technique was used. The first gate is centered on the rising part of the sig-  
 124 nal, while the second one is centered on the maximum amplitude. By plotting  
 125 the correlation of these two charge signals (Fig. 8), the alpha-fission fragment  
 126 separation can be improved from 66% to 91% for the 14.4 MBq  $^{240}\text{Pu}$  sample.

127 Table 1 summarizes the measured efficiencies for the  $^{240,242}\text{Pu}$  samples, in  
 128 different configurations: plain anode, segmented anode, segmented anode and  
 129 PSD analysis. These results show that using the segmented anode and a PSD  
 130 analysis, an efficiency as high as 91% can be obtained. For the lower activity  
 131  $^{242}\text{Pu}$  sample (0.247 MBq), the standard fission chamber provides a very good  
 132 alpha-fission fragment discrimination and the improvements of the detector has  
 133 less impact.

134 These tests validate the new concept of anode developed for high alpha-  
 135 activity actinides used in the fission chamber and new experimental measure-  
 136 ments of  $^{239}\text{Pu}(n,f)$  PFNS were performed at WNR@LANSC (see section 5).

Table 1: *Informations concerning  $^{240,242}\text{Pu}$  tests, with the values of expected and measured fission rates for each isotope. SF stands for Spontaneous Fission.*

<b>Actinide</b>	$^{240}\text{Pu}$	$^{242}\text{Pu}$
Alpha activity (MBq)	14.41	0.247
SF branching ratio	5.7E-8	5.5E-6
SF rate (Hz)	0.82	1.36
Fragment emission efficiency	0.94	0.94
Expected fission rate (Hz)	0.77	1.28
<b>Plain anode</b>		
Measured fission rate (Hz)	0.51	1.24
<b>FF efficiency (%)</b>	<b>66</b>	<b>97</b>
<b>Segmented anode</b>		
Measured fission rate (Hz)	0.60	1.25
<b>FF efficiency (%)</b>	<b>78</b>	<b>98</b>
<b>Segmented anode + PSD</b>		
Measured fission rate (Hz)	0.70	1.27
<b>FF efficiency (%)</b>	<b>91</b>	<b>99</b>

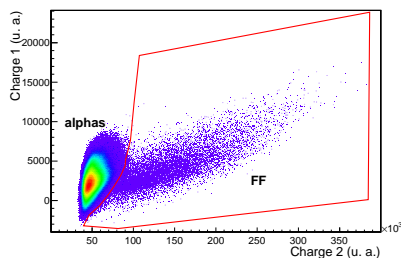


Figure 8: *Example of a 2D histogram showing the alpha-fission fragment discrimination for the  $^{240}\text{Pu}$  sample. This histogram is obtained by plotting one charge integration versus the second one (see text for details).*

#### 137 4. Simulations of the neutrons scattering

138 The NPTool framework [7, 8] using the Geant4 simulation package was  
 139 used to quantify the neutron scattering generated by the structural material  
 140 of the fission chamber. In this work, we used the high precision transport model  
 141 G4NeutronHP using the default G4NDL nuclear data. During experiments, the  
 142 fission chamber is placed at the center of an array of 54 liquid-scintillator cells  
 143 (Chi-Nu cells) as it can be seen in Fig. 9. Both incoming and outgoing neutrons  
 144 may scatter with the air or with the detector materials, inducing neutron back-  
 145 ground in the cells and a distortion of the neutron energy spectra. The detailed  
 146 geometry and material of the fission chamber was carefully included in the sim-  
 147 ulation (anode, cathode, Ti walls, Al frame, PCB...) In order to quantify the  
 148 effect of the fission chamber, two different simulations have been performed: one  
 149 only with air and the second one with the fission chamber included (see Fig. 9).  
 150 Fig. 10 shows the fraction of incoming neutrons scattered either by the air or  
 151 by the fission chamber. The blue points correspond to the first simulation only  
 152 with air while the open red circles show the effect of the added fission chamber.  
 153 One can see that the fission chamber materials add a negligible background to  
 154 the prompt-fission neutrons. Moreover, these prompt neutrons of interest are  
 155 detected in coincidence with a fission, then all scattered neutrons outside the

156 coincidence gate do not affect the measurement. As a consequence the fraction  
 157 of scattered neutrons shown in Fig. 10 corresponds to a higher limit which is  
 reduced by the coincidence gate.

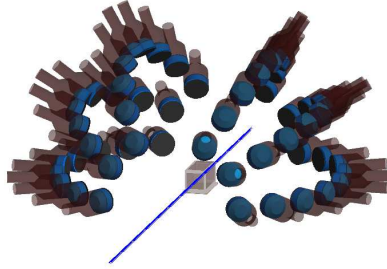


Figure 9: *GEANT4 geometry of the fission chamber used in the NPTool simulations. 54 cells surrounding the fission chamber are reproduced. The incoming neutron beam is represented by the blue trajectories.*

158

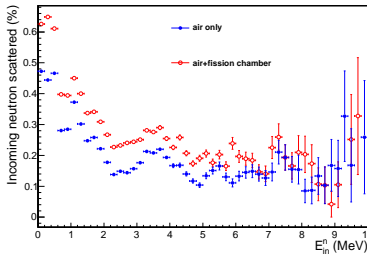


Figure 10: *Normalized incoming neutrons scattered on air (blue full circles) and air+fission chamber (red open circles). A maximum of 0.6% at very low energy of the incoming neutrons are scattered and detected in a Chi-Nu cell, and the effect of the fission chamber is negligible.*

## 159 5. Experimental uses

160  $^{239}\text{Pu}$  Prompt-Fission-Neutron Spectra (PFNS) were measured placing the  
 161 fission chamber, containing 47 mg of actinide in the WNR neutron beam to

162 induce fission of the Pu deposits. The detector was surrounded by the 54 liquid  
 163 scintillator cells of the Chi-Nu array [9]. The incoming-neutron energy is deter-  
 164 mined by time-of-flight measurement between the beam pulsation and the event  
 165 detected in the chamber. Neutrons and gammas emitted by neutron-induced  
 166 fission reaction were detected and identified in the scintillator cells, and neu-  
 167 trons energies measured via time-of-flight technique. Results of this experiment  
 168 were presented in [10]. As an example, Fig. 11 shows the pulse-height spectra of  
 169  $^{239}\text{Pu}$  fission chamber with and without beam. The fission detection efficiency  
 170 was estimated to be close to 95% for 10 MBq alpha activity per channel, thanks  
 171 to some improvements on the design of the front-end electronics boards.

172 This good fission event identification probability, combined the very low  
 173 neutron detection threshold ( $\approx 200$  keV) and the granularity of the Chi-Nu  
 174 detector, allowing angular emission corrections, as well as the high recorded  
 175 statistics, lead to very precise PFNS measurements. Moreover, thanks to these  
 176 characteristics, the number of neutrons emitted per fission ( $\bar{\nu}$ ) as a function of  
 177 incoming energy was extracted from the measurement with an unprecedented  
 178 accuracy [11].

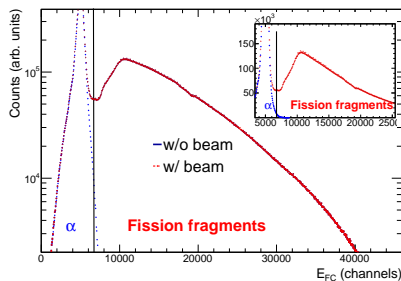


Figure 11: *Pulse height spectra of  $^{239}\text{Pu}$  fission chamber obtained with (red) and without (blue) beam (extracted from [10]).*

## 179 6. Conclusions

180 The fission chamber developed for PFNS measurements was improved to be  
181 used with high alpha-activity samples. The housing was modified to allow the  
182 assembly of the detector in a gloves box. For fission detection, a new concept  
183 of segmented anode was developed. Thanks to the use of these segmented  
184 anodes and modern front-end electronics, a fission detection efficiency of 95%  
185 was reached for alpha activities as high as 10 MBq, to be compared to a fission  
186 rate of 15 f/s.

187 Thanks to its very high alpha-fission fragment discrimination capability, this  
188 fission chamber can be further used in fission cross-section as well as PFNS  
189 measurements of very active actinides, such as  $^{238,240,241,242}\text{Pu}$ .

## 190 References

- 191 [1] J. Taieb, B. Laurent, G. Bélier, A. Sardet, C. Varignon, Nucl. Instr. and  
192 Meth. A 833 (2016) 1–7.
- 193 [2] A. Sardet, C. Varignon, B. Laurent, T. Granier, A. Oberstedt, Nucl. Instr.  
194 and Meth. A 792 (2015) 74–80.
- 195 [3] B. Laurent, P. Marini, G. Bélier, T. Bonnet, A. Chatillon, J. Taieb,  
196 D. Etasse, M. Devlin, R. Haight, EPJ Web Conf. 146 (2017) 04014.
- 197 [4] Torlon, Solvay specialty polymers,  
198 <http://www.solvayplastics.com/>.
- 199 [5] J. Taieb, B. Laurent, Fr. patent 3069700, 2019-02-01.
- 200 [6] L. Mathieu, private communication, 2015.
- 201 [7] A. Matta, P. Morfouace, N. de Séréville, F. Flavigny, M. Labiche, R. Shear-  
202 man, Journal of Physics G: Nuclear and Particle Physics 43 (2016) 045113.
- 203 [8] NPTool, a ROOT/Geant4 based framework for Nuclear Physics,  
204 <https://gitlab.in2p3.fr/np/nptool>, consulted on November 2020.

- 205 [9] R. C. Haight, H. Y. Lee, T. N. Taddeucci, J. M. O'Donnell, B. A. Perdue,  
206 N. Fotiades, M. Devlin, J. L. Ullmann, A. Laptev, T. Bredeweg, M. Jandel,  
207 R. O. Nelson, S. A. Wender, M. C. White, C. Y. Wu, E. Kwan, A. Chyzh,  
208 R. Henderson, J. Gostic, *J. Instrum.* 7 (2012) C03028.
- 209 [10] P. Marini, J. Taieb, B. Laurent, G. Belier, A. Chatillon, D. Etasse, P. Mor-  
210 fouace, M. Devlin, J. A. Gomez, R. C. Haight, K. J. Kelly, J. M. O'Donnell,  
211 K. T. Schmitt, *Phys. Rev. C* 101 (2020) 044614.
- 212 [11] P. Marini, J. Taieb, G. Belier, A. Chatillon, D. Etasse, B. Laurent, P. Mor-  
213 fouace, M. Devlin, J. A. Gomez, R. C. Haight, K. J. Kelly, J. M. O'Donnell,  
214 submitted to *Phys. Rev. Lett.* (Nov. 2020).